Nanoscale Advances

ROYAL SOCIETY OF CHEMISTRY

PAPER

View Article Online
View Journal | View Issue

Cite this: *Nanoscale Adv.*, 2024, **6**, 2113

Silver-deposited titanium as a prophylactic 'nano coat' for peri-implantitis†

Vaibhav Madiwal[ab] and Jyutika Rajwade *[ab]

Dental implant failures caused by bacterial infections are a significant concern for dental implantologists. We modified the titanium surface by depositing silver (Ti-Ag) using direct current (DC) sputtering and confirmed the formation of a 'nano coat' by X-ray photoelectron spectroscopy (XPS), surface profilometry and energy dispersive spectroscopy (EDS). Scanning electron microscopy (SEM) and atomic force microscopy (AFM) revealed the deposition of a uniform nano Ag thin film. A gradual increase in thickness was observed, and the film thickness (530 nm) at 5 min deposition time (Ti-Ag_5) resulted in a reduction of the water contact angle (WCA, 15%) and an increase in surface energy (SFE, 22%) in comparison to the uncoated Ti surface. Using inductively coupled plasma-atomic emission spectroscopy (ICP-AES), the slow, steady release of Ag from the coating was observed over 21 days. The Ti-Ag_5 surface exhibited excellent antibacterial activity against *Streptococcus oralis*, *Streptococcus sanguinis*, *Aggregatibacter actinomycetemcomitans*, and *Porphyromonas gingivalis*, which belonged to the yellow, purple, and red complexes, representing specific periodontal pathogens. Furthermore, we observed excellent cytocompatibility of Ag-deposited Ti towards MG-63 osteoblasts with no inhibitory effect on their proliferative potential. Quantitation of alkaline phosphatase (ALP) activity, mineralization efficiency, and osteogenesis-related gene expression of MG-63 cells over 21 days was suggestive of rapid osseointegration. Overall, the 'nano coat' of Ag on Ti is indeed a prophylactic against peri-implantitis, ensuring increased implant success.

Received 18th October 2023
Accepted 6th March 2024

DOI: 10.1039/d3na00898c

rsc.li/nanoscale-advances

1. Introduction

Dental implants are used worldwide to treat edentulism and form an integral part of modern implant dentistry. In the USA alone, 3 million implants were placed, with an increasing trend indicating ~500 000/annum.[1] The placement of implants in patients is increasing primarily due to a high success rate, which is around 95%.[2] The failures (~5%) can be attributed to host factors such as diabetes, quality and quantity of the surrounding bone, history of periodontitis, harmful habits such as smoking and alcoholism, and bacterial infection.[3] However, it was found that among all the clinical conditions, bacterial infection is a pivotal factor governing peri-implantitis and dental implant failure.[4,5] The microbial community in peri-implantitis infection is mainly populated by *Tannerella forsythia*, *Treponema denticola*, and *Porphyromonas gingivalis*, representing the 'red-complex'.[6,7] In addition, other biomechanical factors such as implant material, geometry, surface structure, and surgical procedures have been shown to affect the implant success rate.[8,9] Despite excellent physicochemical properties, conventional titanium implants require at least three months of a stress-free healing period, which may increase the risk of infection during the initial period, which may lead to implant failure.[10] Additionally, individuals looking forward to a quick restoration of the aesthetic look generally would not accept a long healing period. Therefore, to increase the implant success rate, contemporary research is focused on imparting antimicrobial properties and facilitating the rapid osseointegration of the implant. These goals could be achieved by surface modification of the implant by changing the native surface structure and/or applying a functional coating. More emphasis is given to surface modification using multifunctional compounds with both antibacterial and osseointegrative properties.[11] Two strategies, *viz.*, active or passive coatings and physical modifications, have been used to impart these properties to the inert titanium surface. Active coating relies on the local release of the functional compound from the coating, which performs its effector functions, whereas passive coating shows effects only upon physical contact with bacteria (contact killing) or eukaryotic cells (enhanced attachment and spreading). The physical surface modification of implants includes strategies that change in the native surface properties such as surface roughness, surface energy, chemical properties,

[a]*Nanobioscience Group, Agharkar Research Institute, G. G. Agarkar Road, Pune 411004, India. E-mail: jrajwade@aripune.org; vmadiwal@aripune.org; Tel: +91-020-025325131*

[b]*Savitribai Phule Pune University, Homi Bhabha Road, Pune 411007, India*

† Electronic supplementary information (ESI) available. See DOI: https://doi.org/10.1039/d3na00898c

and wettability to achieve better osseointegration and bacterial killing.[12]

To date, surface modifications using physical (grit blasting, acid etching, laser ablation, *etc.*), chemical (anodization, hydroxyapatite, and UV-photo functionalization, *etc.*) methods and employing biomolecules *viz.*, grafting ECM components, RGD peptide, bactericidal peptides, and antimicrobials, *etc.*, have been reported.[13–15] Several challenges exist for current surface modification technologies; mature commercial technologies sometimes offer only limited functionalities, whereas newly developed technologies impart finer surface properties. The latter is difficult to commercialize due to the higher cost and low stability of the obtained surface.[12] Metals have been used extensively for the surface modification of dental implants owing to their chemical stability, broad-spectrum antibacterial activity, and lower bacterial resistance.[16,17] Sputtering is a widely used technique for the deposition of pure metals and metal alloys thin films on various surfaces to achieve antibacterial properties.[18–21] Grade II Ti deposited with silver nanoparticles using ion implantation, followed by a coating of silver thin film using magnetron sputtering, showed 64.6% antibacterial activity against *S. aureus* with no harmful effect on the dental pulp stem cells (DPSC) after 14 days of incubation.[22] Zn nanowires modified Ti exhibited enhanced cell adhesion, proliferation, and osteogenic differentiation of MC3T3-E1 cells along with good antibacterial activity against *Staphylococcus aureus*, *Porphyromonas gingivalis*, and *Actinobacillus actinomycetemcomitans*.[23] A novel Cu-bearing Ti alloy demonstrated a sustainable bactericidal effect against *Streptococcus mutans* and *Porphyromonas gingivalis* without a cytotoxic effect on rBMSCs.[24]

A previous study from our laboratory demonstrated that nanoscale silver deposition on titania abutments inhibited pathogenic microorganisms, such as *Pseudomonas aeruginosa*, *Streptococcus mutans*, *Staphylococcus aureus*, and *Candida albicans*, and exhibited good cytocompatibility against primary human gingival fibroblasts.[25] The study was aimed at restricting bacterial attachment on the abutment surface, which is considered an entry point for the bacteria to gain access to the implant surface. As an extension of previous work, the current study focuses on the deposition of Ag on Ti using DC sputtering. The novelty of this study is that we assessed the antibacterial potential of Ag-deposited Ti against specific periodontal pathogens implicated in peri-implantitis. An Indian strain, *Porphyromonas gingivalis 93*, was included in addition to periodontal pathogens. Furthermore, the effects of the Ag-deposited Ti on the biological activities of bone forming cells (MG-63 osteoblast) were evaluated as an indication of osseointegration.

2. Experimental procedures

2.1. Fabrication of Ag-deposited Ti

Ti-6Al-4V alloy polished discs with 10 mm diameter and 2 mm thickness (Bhagyashali metal, Mumbai, India) were used in this study. The 'as received' discs were cleaned using a warm detergent solution, followed by five water washes and drying in the oven. Then, the discs were washed with acetone, isopropanol, and ultra-pure water successively for 15 min each in the ultrasonic water bath, followed by drying in the oven. Silver (Ag) was deposited on Ti discs using a DC sputtering machine (Hind HiVac, Bangalore, India). Briefly, Ag foil (99.99% pure, diameter 3″, thickness 0.2 mm) was used as a target with a fixed target to the substrate (Ti discs) distance of 3 cm. The deposition of Ag was carried out in the presence of an argon plasma atmosphere (100 mA direct current and 0.1 mbar working pressure) for varying time intervals of 1, 2, and 5 min. Ag-deposited Ti discs were abbreviated as Ti-Ag_1, Ti-Ag_2, and Ti-Ag_5, respectively. The undeposited Ti discs were used as a control sample.

2.2. Surface morphological and topological analysis

The analysis of surface morphology and elemental composition of the Ti and Ag-deposited Ti samples was performed using a scanning electron microscope (SEM, MA15 EVO®; Carl Zeiss, Germany) coupled with EDS (Oxford Instruments, Abingdon, UK). Before analysis, the samples were sputter coated with a gold thin film, and the images were captured at an accelerating voltage of 20 kV.

The surface topology and roughness of the samples were also measured using atomic force microscopy (AFM) (Innova®, Bruker, Massachusetts, USA). An antimony-doped silicon tip (resonance frequency of 300 kHz and nominal elastic constant of 40 N m^{-1}) was employed to scan the surface in tapping mode. Gwyddion software (a freeware for scanning probe microscopy) was used to view and analyze AFM images. The roughness average (Ra), which is the arithmetic mean of the absolute values of the height deviations from the mean line, was considered for the analysis.

The coating thickness and sputter deposition rate of the Ag thin film were calculated using a surface profilometer. For thickness analysis, initially half of the Ti disc surface was masked with Kapton® tape, and Ag deposition was carried out for 15 min. After deposition, the tape was carefully removed, and the samples were scanned across the surface (indicate area scanned) to obtain the step height profile of the thin film. The deposition rate was calculated by dividing the total thickness (in nm) by the deposition time and was reported as nm min^{-1}.

2.3. Total metal content and ion release study

The quantitative estimation of the total Ag deposited on Ti discs was estimated using AAS (ContrAA 800D, Analytikjena, Germany). As described by Kheur *et al.*,[25] each sample was immersed separately in 1 mL of concentrated nitric acid for 12 h. The acid solution was then diluted up to 10 mL using double distilled water in the standard flask and used directly for estimation. The amount of Ag deposited was expressed as the absolute concentration of Ag per unit area of the Ti disc.

The release profile of Ag ions from the Ti-Ag_5 sample was monitored in the phosphate-buffered saline (PBS, 10 mM, pH 7.2). For this, initially, each sample was immersed in 1 mL of PBS in a 24-well plate and incubated at 37 °C for predetermined time points *viz.*, 0, 1, 3, 7, 14, 21, and 28 days. At the end of each

time point, the solution was collected separately in micro-centrifuge tubes and replaced with 1 mL of fresh PBS, and the plate was re-incubated. Each sample was digested with concentrated nitric acid for 12 h, which was suitably diluted using double distilled water, and analyzed by inductively coupled plasma-atomic emission spectroscopy (ICP-AES) (ARCOS, SPECTRO analytical instruments GmbH, Germany).

2.4. Wettability study

The wettability and surface energy of the Ti and Ag-deposited Ti samples were determined using CA measurements. The CA measurements were carried out using a drop shape analyzer (DSA25S, Kruss Scientific, Hamburg, Germany) instrument in static mode using double distilled water and di-idomethan as a wetting medium (2 μL) at room temperature (RT). The representative contact angle is the mean of three independent measurements. The surface free energy was calculated using the Owens–Wendt geometric mean equation (eqn (1)):[26]

$$\gamma_L(1+\cos\theta) = 2\sqrt{\gamma_S^D\gamma_L^D} + 2\sqrt{\gamma_S^P\gamma_L^P}, \quad (1)$$

where θ is the measured contact angle, γ_L is the surface tension of the liquid, and γ_L^D and γ_L^P are dispersive and polar components of the liquids, respectively. The surface free energy [$\gamma_S = \gamma_S^D + \gamma_S^P$] was determined by measuring the CA of water and di-idomethan.

2.5. Nanomechanical properties

The nanomechanical properties, such as hardness and elastic modulus of the Ag coating (Ti-Ag_5 surface), were assessed by nanoindentation using a G200 Nano Tester (Agilent, California, United States) equipped with a Berkovich diamond indenter for continuous stiffness measurements. A maximal load of 2 mN was applied on the surface, 6 indentations were made on the randomly selected area, and corresponding force–displacement curves were recorded.[27] The average hardness (H) and Young's modulus (E) were determined from the slope of the unloading force–displacement curve based on the relationship described by Oliver and Pharr.

2.6. Surface chemical composition

The surface chemical composition of the Ti and Ti-Ag_5 was analyzed using XPS (ESCALAB Xi+, Thermo Fisher Scientific, UK). A monochromatic Al Kα X-ray source was used to irradiate the samples (Spot size 900 μm diameter). The survey spectra (0–1350 eV) were acquired at pass energy (CAE) of 200 eV and step size of 1.0 eV, whereas a narrow scan of Ag 3d was acquired at pass energy (CAE) of 50 eV and step size of 0.1 eV. The ultra-high vacuum in the preloc and analysis chambers was maintained at 7×10^{-9} and 5×10^{-10} mbar, respectively. Spectral data processor (SDP v8.0) software was used to analyze the survey spectra and deconvolution of the peaks.[25]

2.7. *In vitro* antibacterial assays

The antibacterial assays were performed using periodontal pathogens, *viz.*, *Streptococcus oralis* ATCC 6249 (So), *Streptococcus sanguinis* ATCC 10556 (Ss), Aggregatibacter actinomycetemcomitans ATCC 29522 (Aa), *Porphyromonas gingivalis* ATCC 33277 (Pg), and *Porphyromonas gingivalis* 93 (Pg93) (Indian strain). Ss and So were grown and maintained in brain heart infusion broth and agar aerobically. Aa was grown anaerobically in thioglycollate broth and tryptic soy-serum bacitracin vancomycin (TSBV) agar. The Pg strains were grown anaerobically in ATCC medium 2722 and Columbia blood agar (supplemented with 5% sheep blood). All the cultures were incubated at 37 °C. Before every antibacterial and cell culture assay the native Ti and Ag-deposited Ti samples were surface sterilized on both sides using ultraviolet radiation (30 min on each side).

The antibacterial activity of the Ti-Ag samples was assessed using the modified Japanese Industrial Standards (JIS Z 2801:2000) method. For this, 0.1 OD (600 nm) bacterial stock suspensions (approx. 10^8 cells per mL) were prepared in respective broth medium. An aliquot (50 μL) containing $\sim 10^5$ cells was inoculated onto each sample and covered with a sterile plastic thin film. The samples were incubated in a humidified chamber at 37 °C for 24 h. After incubation, the inoculated discs were aseptically transferred to 1 mL of sterile PBS, vortexed vigorously, and sonicated for 2 min. 10-fold serial dilutions from these suspensions were prepared, and 10 μL of each dilution was spot inoculated on the respective agar medium and incubated at 37 °C. The antibacterial activity of the Ag-deposited Ti was determined by calculating the reduction in bacterial number (CFU mL^{-1}) compared to the Ti using the following formula (eqn (2)):

$$\text{Antibacterial activity}(\%) = \frac{\text{CFU of control surface} - \text{CFU of treatment surface}}{\text{CFU of control surface}} \times 100. \quad (2)$$

A qualitative assessment of the anti-adhesive activity of Ag-deposited Ti samples was performed using live–dead staining. For this, 1 mL of bacterial suspension was inoculated on each pre-sterilized sample and incubated at the conditions mentioned earlier for 24 h. After incubation, the samples were gently washed with PBS to remove loosely attached cells. The biofilm was stained with SYTO 9 (2.5 μM, 480/500, green fluorescence) and propidium iodide (PI) (20 μM, 560/635, red fluorescence) dyes, which were labeled as live and dead cells, respectively. The samples were incubated at room temperature for 30 min under dark conditions. Later, the excess stain was washed off with PBS, and the samples were observed under a confocal laser scanning microscope (CLSM) (TCS SP8, Leica, Wetzlar, Germany). 10% glycerol was used as a mounting medium to avoid drying samples during imaging.

Another set of samples was prepared as described above and after incubation. All the discs were washed with PBS, and the cells were fixed in 2.5% glutaraldehyde solution for 1 h at RT. Excess glutaraldehyde was aspirated, and the samples were washed twice with PBS. The samples were then sequentially dehydrated in an ethanol gradient (50, 70, 80, 90, 95, and 100%, 10 min incubation for each treatment). After dehydration, the samples were sputter coated with gold and observed under SEM.

2.8. *In vitro* cell culture assays

For the cell culture study, the MG-63 osteosarcoma cell line (P-30 to P-40) was used. The cells were cultured in α- MEM supplemented with 10% FBS and 1% antibiotic and antimycotic solution in a 25 cm^2 tissue culture flask at 37 °C, 5% CO_2, and 95% relative humidity. To facilitate cell attachment only to the sample surface, initially, 80 μL of cell suspension was seeded onto the sample, followed by incubation for 2 h at 37 °C, 5% CO_2, and 95% relative humidity. 1 mL of fresh medium was added to each sample and incubated further for predetermined time points. This cell seeding procedure was followed for all the cell culture experiments.

The cytotoxicity of the Ag-deposited Ti samples was assessed using MTT (3-(4,5-dimethylthiazol-2-yl)-2-5 diphenyl tetrazolium bromide) (USB, Cleveland, USA) assay. 4×10^4 cells were seeded on each sample placed in a 24-well plate and incubated for 24 h. After incubation, an MTT solution (stock concentration, 5 mg mL^{-1}) was added to each well and further incubated for 4 h. The formazan crystals were then dissolved in dimethyl sulfoxide, and the absorbance of the resultant solution was recorded at 570 nm using a multi-well plate reader (Synergy HT, Bio-Tek Instruments Inc., USA). For the cell proliferation assay, 2×10^4 cells were seeded on all the samples in a 24-well plate and incubated at 37 °C in a humidified atmosphere of 5% CO_2 for 3, 5, and 7 days (fresh media replenished every two days). After completion of each incubation time, a procedure similar to that of the cell viability assay mentioned above was repeated. The percentage cell viability was calculated using the following formula (eqn (3)):

$$\text{Cell viability } (\%) = \frac{\text{OD}_{570\text{ nm}} \text{ treatment group}}{\text{OD}_{570\text{ nm}} \text{ control group}} \times 100. \quad (3)$$

Confocal laser scanning microscopy (CLSM) was used to observe cell adhesion and cytoskeletal architecture of the MG-63 cells grown on Ti and Ti-Ag samples. For this, 2.5×10^4 cells were seeded on each sample kept in a 24-well plate and incubated at 37 °C in a humidified atmosphere of 5% CO_2 for 24 h. Before staining, the samples were washed with PBS and fixed using 4% paraformaldehyde (PFA) for 15 min, followed by permeabilization in 0.1% Triton X-100 for 5 min. The actin cytoskeleton was visualized under CLSM after staining with rhodamin-phalloidin (Invitrogen™, US) for 30 min, and the nucleus was stained with Hoechst dye (Invitrogen™, US) for 10 min. Before observation, excess stains were removed with PBS.

Intracellular ALP activity of MG-63 osteoblast cultured on Ti and Ag-deposited Ti samples was monitored by enzymatic conversion of *p*-nitrophenol phosphate (pNPP) to yellow-colored *p*-nitrophenol spectrophotometrically. For this, 2×10^4 cells were inoculated on each sample kept in a 24-well plate and incubated at 37 °C in a humidified atmosphere of 5% CO_2 for 7 and 14 days (fresh media was added every two days). On days 7 and 14, the cells were lysed in RIPA buffer (Himedia, Mumbai, India) for 1 h at 4 °C. The lysates were centrifuged at 12 000 rpm for 20 min at 4 °C, and the supernatants were collected in fresh tubes. Then, 50 μL of lysate was added to 100 μL of pNPP (10 mM in tris buffer, pH 9, and supplemented with 1 mM $MgCl_2$) solution in a 96-well plate and incubated at 37 °C for 30 min. Finally, the absorbance of yellow-colored *p*-nitrophenol was recorded at 405 nm. The ALP activity was normalized by the total protein content estimated using the BCA assay.

The mineralization efficiency of MG-63 cells cultured on Ti and Ag-deposited Ti was examined using an Alizarin red S (ARS) assay. 2×10^4 cells were seeded on each sample and allowed to grow in normal α-MEM till monolayer formation (6 days). Subsequently, the normal growth medium was replaced with an osteogenic medium (α-MEM supplemented with 50 μg mL^{-1} ascorbic acid, 10 mM β-glycerophosphate, and 100 nM dexamethasone) in which the cells were cultured for 14 and 21 days. On 14 and 21 days, the monolayer was washed with PBS and fixed in 4% PFA for 15 min. The excess PFA was removed by distilled water, and the fixed monolayer was stained with ARS dye (40 mM, 500 μL, pH- 4.2) for 20 min at RT. The residual ARS was removed by thoroughly washing the surface with water, and the stained monolayer was observed under a stereomicroscope (Leica M205A, Wetzlar, Germany). For quantitation, stained monolayers were stored at −20 °C. The dye was extracted in 500 μL of 10% (w/v) cetylpyridinium chloride solution for 1 h; then, the absorbance of the colored solution was recorded at 620 nm.[28]

Quantitative real-time polymerase chain reaction (qRT-PCR) was used to analyze the relative gene expression of the osteogenesis-related genes *viz.*, *ALP*, *Col1α*, *BMP-2*, and *RUNX-2*. The sequences of the forward and reverse primers used are listed in Table S1.† Glyceraldehyde 3-phosphate dehydrogenase (*GAPDH*) was used as the reference gene. To study the gene expression analysis initially, MG-63 cells were cultured on Ti and Ag-deposited Ti for 14 and 21 days, as mentioned earlier. After incubation, the total RNA was extracted using TRIzol reagent (Invitrogen Life Technologies, Carlsbad, CA, USA) as per the manufacturer's protocol. Subsequently, the complementary DNA (cDNA) was synthesized from 1 μg of total RNA using a ReadyScript® cDNA synthesis kit (Sigma-Aldrich, St. Louis, United States). The qPCR was performed using LightCycler® 480 SYBR Green I Master mix on the LightCycler®480 platform (Roche Diagnostics, Switzerland). The qPCR cycles consist of an initial denaturation step at 94 °C for 5 min, followed by 40 amplification cycles consisting of 94, 58, and 72 °C for 10, 30, and 30 seconds. Gene expression was studied using the comparative $2^{-\Delta\Delta CT}$ method according to Livak and Schmittgen (2001).[29] Threshold values (C_T) generated from the software tool (Roche LC 2.0) were employed to quantify relative gene expression.

2.9 Hemolysis assay

The hemocompatibility of the samples was determined as per the procedure described by Patil *et al.*[30] Briefly, freshly drawn sheep blood was centrifuged at 500×*g* to concentrate the RBCs. The RBC pellet was washed with normal saline until a clear supernatant appeared. The concentrated RBCs were diluted with saline (1 : 9), and 500 μL of diluted RBC suspension was

added to the Ti and Ag-deposited Ti samples and incubated at 37 °C for 1 h. After incubation, the RBC suspension was collected in a fresh microcentrifuge tube and centrifuged at 500×*g* for 5 min. Following this, Drabkin's reagent was added, and the cyanmethemoglobin formed was estimated by recording the absorbance at 540 nm using a multi-well plate reader (SynergyHT, Biotek, USA). Saline and Triton X-100 (0.1%, 50 μL) were negative and positive controls, respectively. Percentage hemolysis was calculated using the following formula (eqn (4)):

$$\text{Hemolysis } (\%) = \frac{\text{OD}_{\text{test}} - \text{OD}_{\text{negative control}}}{\text{OD}_{\text{positive control}} - \text{OD}_{\text{negative control}}} \times 100. \quad (4)$$

2.10 Statistical analyses

All the experiments were performed in triplicate. The data are represented as the mean ± standard deviation. One and two-way ANOVA was applied to the data set, followed by the Bonferroni post hoc test to estimate the statistical significance between the control and test groups using GraphPad Prism 5 software. $P < 0.05$, 0.01, and 0.001 were considered statistically different, significant, and highly significant, respectively.

3. Results and discussion

3.1. Material characterization

The morphological features of the Ti and Ag-deposited Ti samples were analyzed using SEM (Fig. 1a–d). The SEM image of the Ti surface (Fig. 1a) showed a rough surface with microscale scratches arranged parallel to each other, which might have been generated during the polishing process. Sputter deposition of Ag resulted in a change in the surface morphology of the native Ti surface. The SEM image of the Ti-Ag_1 surface showed that the Ag nanograins were distributed evenly over the entire surface (Fig. 1b). However, Ti-Ag_2 and Ti-Ag_5 samples showed uniform Ag thin film probably formed by coalesces of the discrete Ag nanograins (Fig. 1c and d). Additionally, a uniform, smooth Ag thin film was observed at a higher deposition time (Ti-Ag_5) (Fig. 1d) probably formed by the filling of surface irregularities by the Ag thin film. The EDS analysis was employed to confirm the deposition of Ag on the Ti surface. The amounts of Ag deposited on Ti-Ag_1, Ti-Ag_2, and Ti-Ag_5 samples were 0.23, 0.99, and 1.62 weight%, respectively (Table S2†). The EDS results demonstrated an increase in Ag concentration with a corresponding increase in deposition time, which indicates a successful deposition process.

AFM is one of the most widely used techniques to study the topological features of thin films at the nanoscale level. Fig. 1e–h represents the AFM images of the Ti and Ag-deposited Ti samples. The AFM image of Ti (Fig. 1e) also showed rough surface topography, similar to the SEM analysis. The AFM image of the Ti-Ag_1 showed the presence of evenly distributed Ag nanograins (Fig. 1f), whereas coalescence of the Ag nanograins was evident in the AFM images of Ti-Ag_2 and Ti-Ag_5 samples, which resulted in the formation of uniform Ag film (Fig. 1g and h). Further, AFM was used to determine the average surface roughness (Ra) of the samples. The average Ra values for the Ti, Ti-Ag_1, Ti-Ag_2, and Ti-Ag_5 samples were 9.7, 3.4, 2.85, and 1.8 nm, respectively (Fig. 1i). The gradual reduction in Ra with the increase in deposition time indicated the formation of smoother thin films on the rough native Ti surface. The overall reduction in the Ra with the increase in deposition time could be attributed to filling the valleys present on the native Ti surface with Ag film, resulting in the reduction of net peak to valley distance. It has been reported that the surface nano topography of biomaterials provides mechanical cues that regulate an array of cell behaviors, such as attachment, proliferation, migration, and differentiation.[31,32]

Fig. 1l shows the step height profile of the Ag thin film deposited on the Ti disc. 15 min Ag deposition resulted in the formation of approx. 1599 nm film on the Ti disc. Therefore, the Ag sputter deposition rate was calculated to be ∼106 nm min^{-1}; hence, the probable Ag thin film thicknesses on Ti-Ag_1, Ti-Ag_2, and Ti-Ag_5 were 106, 212, and 530 nm, respectively.

A quantitative estimation of the total Ag content of the Ag thin films was performed using AAS. The total Ag deposited on Ti-Ag_1, Ti-Ag_2, and Ti-Ag_5 samples was 6.6, 26, and 81 μg mm^{-2} of Ti disc, respectively (Fig. 1j). The AAS data demonstrated an increase in Ag content with deposition time, which is in good agreement with the EDS results, further proving a proper deposition process. The Ag ion release profile from the Ti-Ag_5 surface in PBS is illustrated in Fig. 1k. The release study was conducted for 28 days to assess the long-term release pattern. A slow, sustained release of Ag was observed for up to 21 days. Such long-term release of Ag would ensure a reduction in post-operative bacterial infection and support the natural healing of the implant for successful osseointegration.[33]

The surface wettability of biomaterial plays a crucial role in the initial adsorption of serum proteins, which further decides the fate of cell attachment, proliferation, and differentiation processes.[34] Fig. 2a shows the results of the WCA measurement (red bars: the image of water droplets formed on respective samples are shown on top of the bar) for all the samples. The native Ti surface showed an average WCA of 85°, whereas the WCA for Ti-Ag_1, Ti-Ag_2, and Ti-Ag_5 samples were 34, 52, and 72°, respectively. A significant reduction in the WCA was observed after Ag deposition, which could be attributed to the nanoscale surface changes that occurred on the deposited samples. The SFE values calculated using the Owens–Wendt geometric mean equation for the Ti, TiAg_1, Ti-Ag_2, and Ti-Ag_5 samples were 37, 68, 57, and 45 mN m^{-1}, respectively (Fig. 2a, blue bars).

The nanoindentation technique is used to measure the nanomechanical properties, such as hardness and elastic modulus of thin coatings on biomaterials.[35] It is used to evaluate hydroxyapatite, TiN, TiB, and Cu–Ag coatings on the Ti surface.[27,35–37] Fig. 2b shows the load–displacement curves obtained from loading and unloading the Berkovich indenter onto the Ti-Ag_5 surface. The average hardness and elastic modulus observed for the Ti-Ag_5 surface were 30.9 and 394.7 GPa, respectively (Table S3†). It is a prerequisite condition for the surface coatings applied to the biomaterials to possess high mechanical properties to ensure their stability during clinical

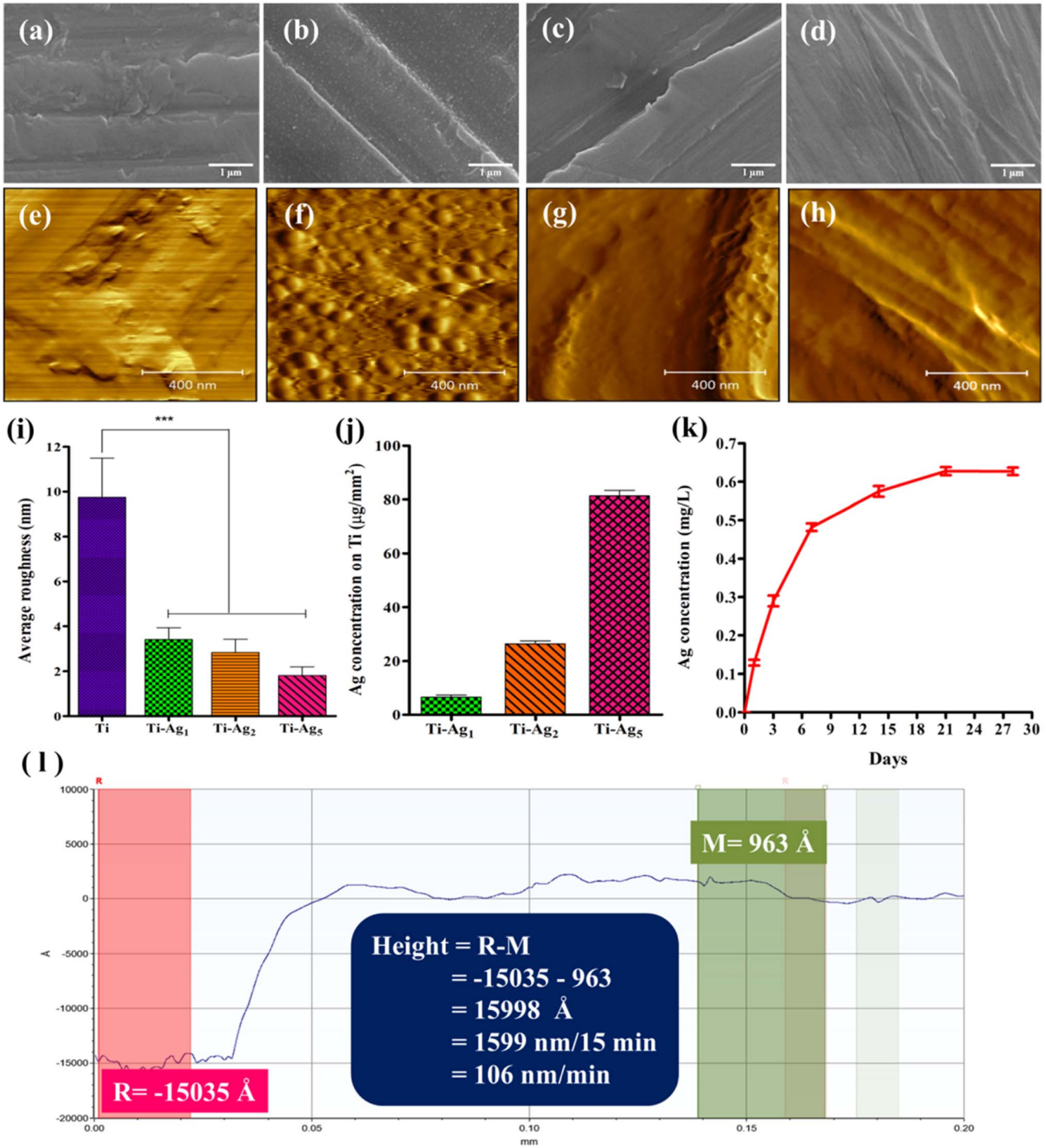

Fig. 1 Scanning electron microscopy images of (a) Ti, (b) Ti-Ag_1, (c) Ti-Ag_2, and (d) Ti-Ag_5. The scale bar represents 1 µm. Atomic force microscopy images of (e) Ti, (f) Ti-Ag_1, (g) Ti-Ag_2, and (h) Ti-Ag_5. The scale bar represents 400 nm. (i) Average surface roughness of Ti and Ag-deposited Ti discs; *** indicates $p < 0.001$ when compared with Ti. (j) Quantitative estimation of the total Ag content deposited on the Ti discs. (k) Evaluation of Ag ion release from Ti-Ag_5 surface over 28 days. (l) Step height profile of 15 min Ag-deposited Ti disc acquired using a profilometer.

use.[27] The data showed the formation of a hard Ag thin film on the Ti surface, which would resist mechanical damage during implantation.

The surface chemical composition of the Ti and Ti-Ag_5 samples was evaluated using XPS. Fig. 2c illustrates the XPS survey spectra acquired from native Ti and Ti-Ag_5. The Ti survey spectrum (red line) showed peaks at 459 and 531 eV, which could be assigned to Ti 2p and O 1s, respectively. The C 1s peak at 285 eV might have originated from the adsorbed hydrocarbons on the surface. The XPS survey spectrum of the Ti-Ag_5

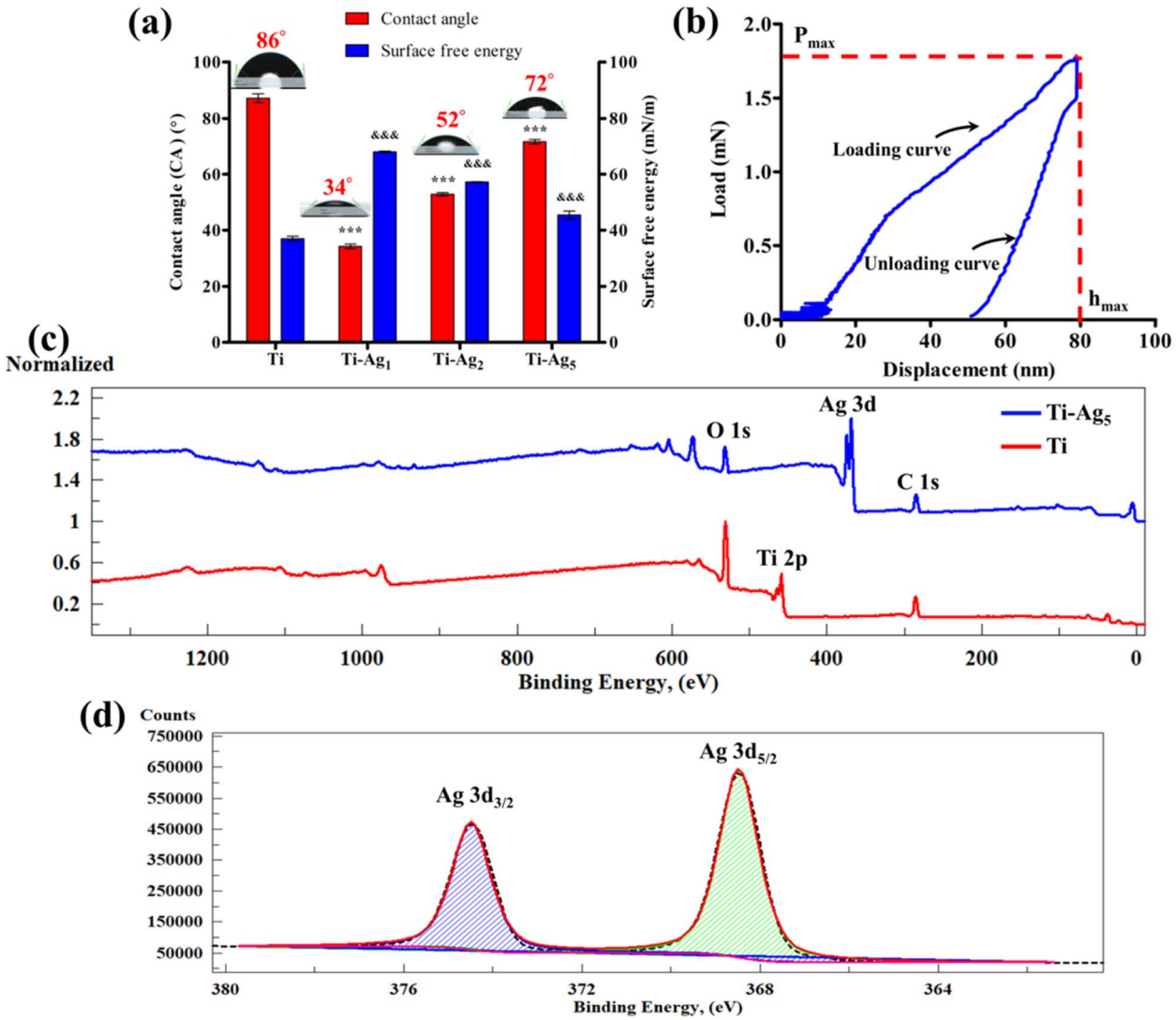

Fig. 2 (a) Assessment of the WCA and SFE of the Ti and Ag-deposited Ti discs. *** and &&& indicate $p < 0.001$ when compared with Ti. (b) Force–displacement curve of Ti-Ag_5 surface obtained using the nanoindentation technique. (c) XPS survey spectra of Ti (red line) and Ti-Ag_5 (blue line). (d) High-resolution deconvoluted Ag 3d spectra.

(blue line) surface showed characteristic peaks of Ag 3d doublet at 368 and 374 eV. In addition, peaks for O 1s and C 1s were observed. The Ti-Ag_5 survey spectrum did not show a characteristic Ti 2p peak due to the deposition of uniform Ag thin film and the depth sensitivity of the XPS analysis. The high-resolution XPS spectrum of the Ag 3d doublet of the Ti-Ag_5 sample is shown in Fig. 2d. The two distinct peaks at 368.5 and 374.5 eV with 6 eV separation correspond to Ag 3d doublet ($3d_{5/2}$ and $3d_{3/2}$, respectively) which confirms the presence of zero valent metallic Ag (Ag^0) in the Ti-Ag_5 samples.[25,38]

3.2. *In vitro* antibacterial activity

The quantitative assessment of the antibacterial activity of Ag-deposited Ti discs was evaluated against periodontal pathogens by applying the modified JIS Z 2801 method. Results of the total viable count (TVC) analysis are presented in Fig. 3. It is worth noting that the Ti-Ag_5 sample exhibited excellent

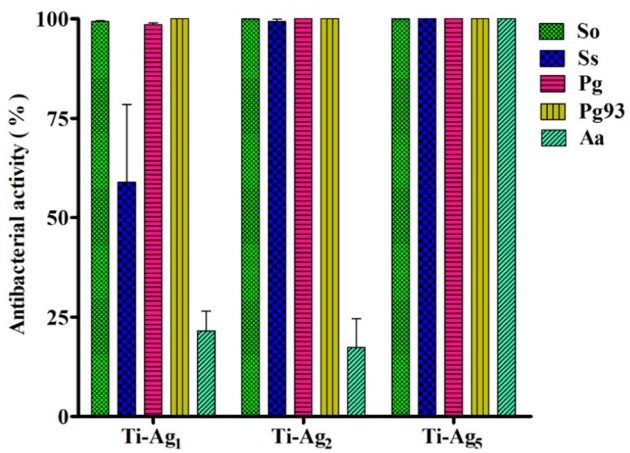

Fig. 3 Antibacterial activity of Ag-deposited Ti samples against periodontal pathogens.

antibacterial performance with >99.999% antibacterial activity against So, Ss, Pg, Pg 93, and Aa. Moreover, the Ti-Ag_2 surface showed >99.999% antibacterial activity against tested pathogens, except for Aa (17%). TVC assay revealed the concentration-dependent killing of pathogens in the order of Ti-Ag_5 > Ti-Ag_2 > Ti-Ag_1. Ti-Ag_1 surface showed the least and most varied antibacterial activity against the tested pathogens, which can be explained by the (a) lower Ag content on the surface and therefore a lesser release from the surface and (b) differences in the nature of the microorganism, *i.e.* species and strain level differences in silver tolerance.

A qualitative assessment anti-adhesive activity of Ag-deposited Ti samples was performed using live–dead fluorescence staining. The native Ti surface showed a large volume of live bacteria (green fluorescence) adhered to the surface, indicating that Ti does not have antibacterial potential (Fig. 4). However, the Ti-Ag_5 surface demonstrated a significant reduction in bacterial cell numbers compared to Ti, Ti-Ag_2, and Ti-Ag_1 after 24 h of incubation. The anti-adhesive activity data further support the TVC assay results, hinting at contact killing of the bacteria due to Ag released from the surface and the modified surface topology.

Fig. 5 shows SEM images of periodontal pathogens grown on Ti and Ag-deposited samples. SEM imaging revealed that native Ti supported the growth of bacteria and that many cells were attached to the surface. On the contrary, the Ti-Ag_5 surface showed a significant reduction in bacterial cell population compared to the control. In addition, the Ti-Ag_5 surface clearly showed a change in bacterial cell morphology and cell surface damage. In comparison, Ti-Ag_2 and Ti-Ag_1 samples showed a marginal reduction in bacterial cell numbers compared to Ti. The release of Ag ions at high concentrations may be responsible for the significant reduction in bacterial cells on the Ti-Ag_5 surface, making the surface unfavorable for bacterial cell attachment. XPS results showed the presence of Ag^0 in the coating. In the past, zerovalent Ag nanoparticles showed potent antibacterial activity against *Staphylococcus aureus*.[39] It has been reported that metal ions exhibit antibacterial activity through the following various mechanisms: (1) direct interaction with sulfhydryl groups of enzymes and proteins and therefore their

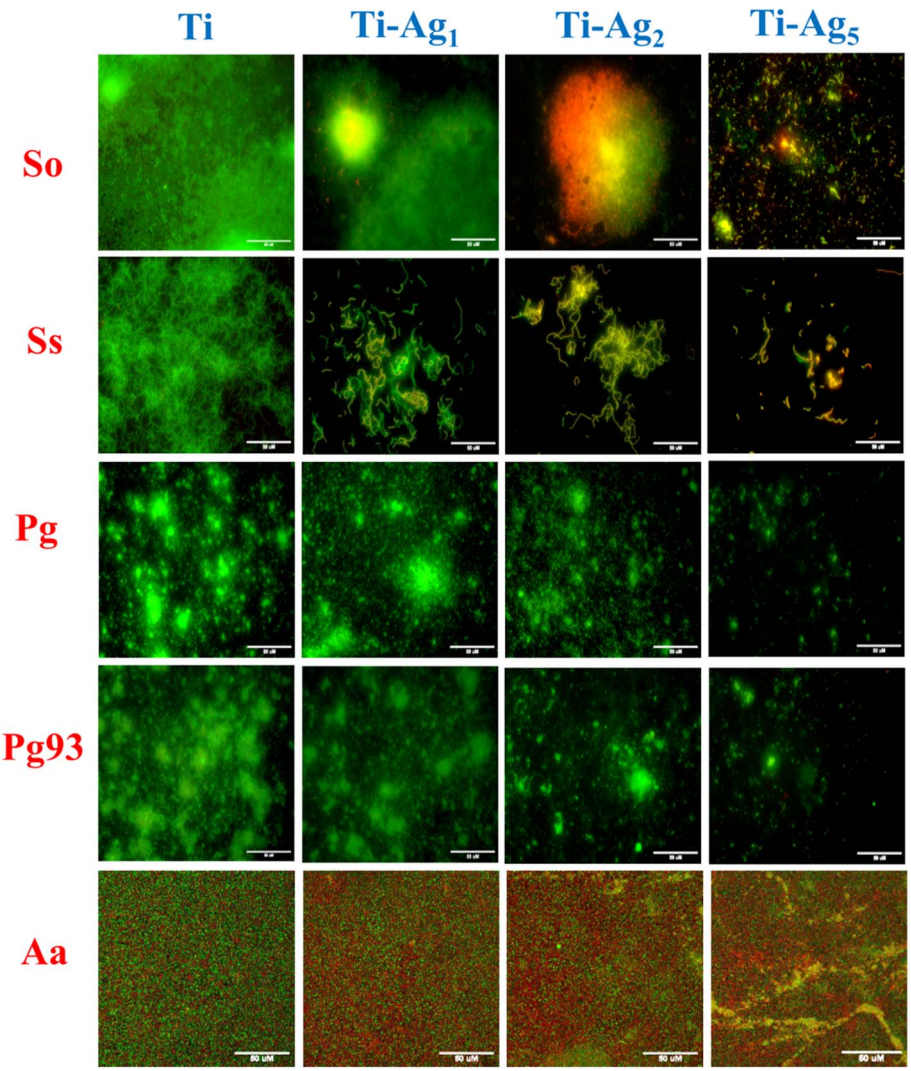

Fig. 4 Live–dead staining of periodontal pathogens grown on Ti and Ag-deposited Ti discs. The scale bar represents 50 μm.

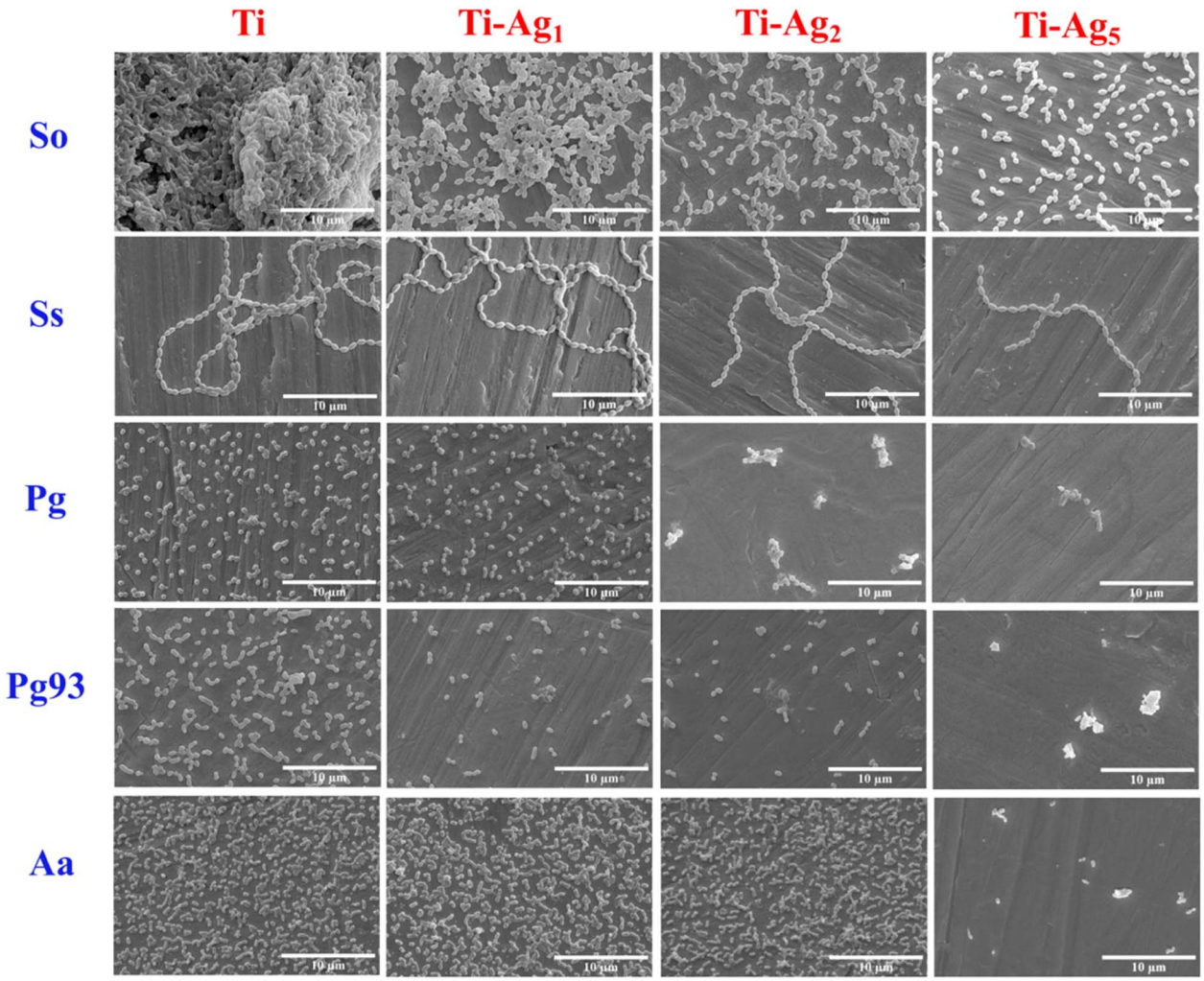

Fig. 5 Scanning electron microscopy images of periodontal pathogens grown on Ti and Ag-deposited Ti discs. The scale bar represents 10 μm.

destabilization. (2) Interaction with transmembrane proteins involved in ATP generation and ion transport; (3) form complex with nucleic acid by intercalating in purine pyrimidine base pairs and disturb H-bond and prevent cell division (4) generation of reactive oxygen species, which causes severe damage to protein, nucleic acid, and lipids, leading to cell death.[40,41] Overall, live–dead staining and SEM substantiate the TVC data.

3.3. *In vitro* biocompatibility

Osteoblasts are the key players in the osseointegration of dental implants. In the past, bone cell culture models have been successfully used to study bone-biomaterial interaction. Various cell lines, such as MC3T3-E1, MG-63, SaOS2, and osteoblast, from human trabecular bone have been routinely used to study the biocompatibility of biomaterials.[42] In this study, we used MG-63 osteosarcoma cells to evaluate the bioactivity of Ag-deposited Ti samples. The antibacterial assay results indicated that Ag-deposited Ti possesses excellent antibacterial activities; however, it is of prime importance to assess the effect of Ag on osteoblast bioactivities. Fig. 6a displays the results of the cell viability assay after 24 h of incubation. From the results, it can be concluded that the Ag-deposited Ti samples did not have any cytotoxic effect on the MG-63 cells. However, Ti-Ag_1 and T-Ag_2 showed slightly increased cell viability compared to native Ti, which suggests that these samples are more favorable for cell attachment and growth.

The effect of the Ag coating on the proliferation potential of Mg-63 cells was assessed using MTT assay at the following predetermined time points: 3, 5, and 7 days. Fig. 6b shows the results of the proliferation assay; a steady increase in cell proliferation over time was observed on all sample samples. No significant difference in the proliferation rate was observed between the groups at each time point, indicating healthy cell growth and good cytocompatibility of the Ag-deposited Ti samples.

Cell adhesion and spreading behavior of MG-63 cells on the Ti and Ag-deposited Ti samples were observed using actin cytoskeleton and nucleus staining. Fig. 6c and d represents the CLSM images of MG-63 cells cultured on Ti and Ag-deposited Ti for 24 h. Cells cultured on the Ti, Ti-Ag_1, and Ti-Ag_2 samples exhibited flat polygonal morphology, and direct cell–cell contact was established. The difference in the number of cells (MTT

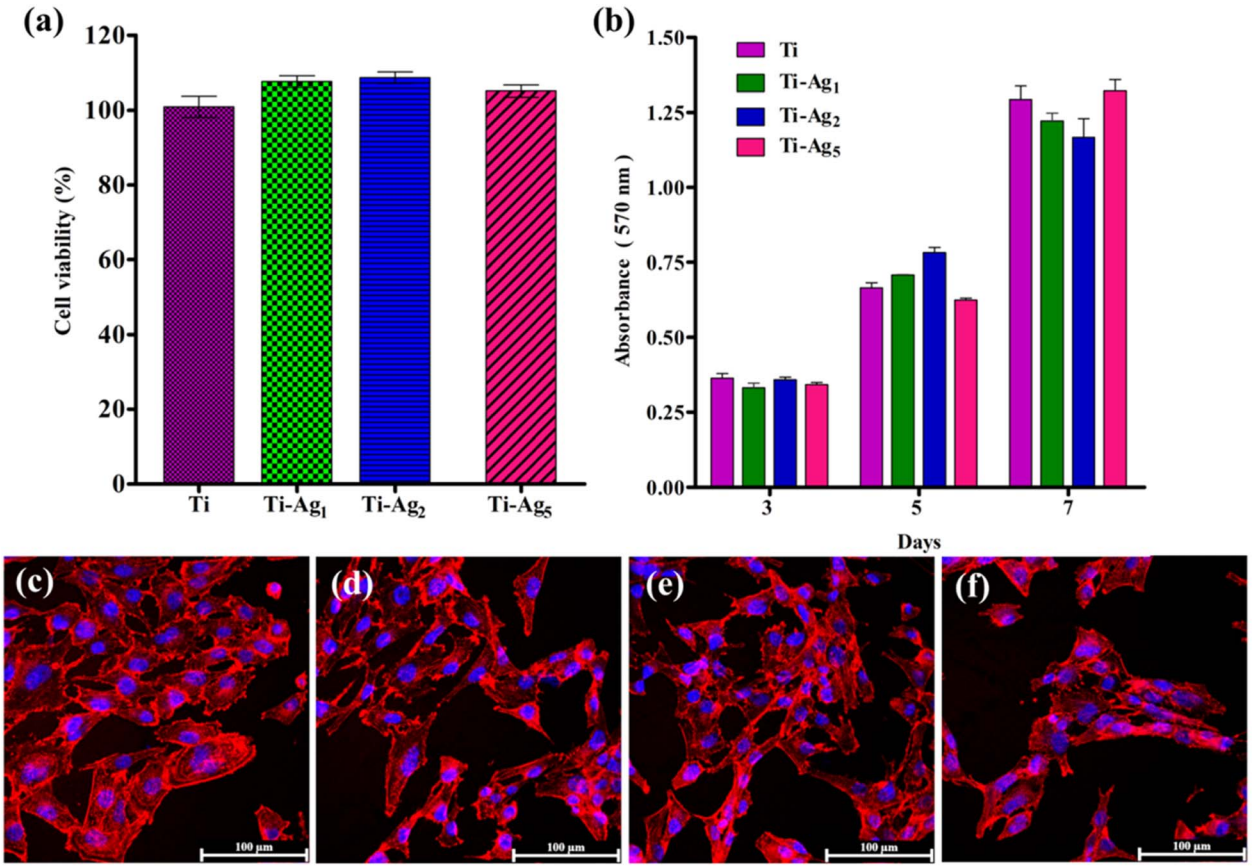

Fig. 6 (a) Percentage cell viability and (b) cell proliferation ability of MG-63 cells cultured on Ti and Ag-deposited Ti discs. Confocal microscopic images of the cytoskeleton and nuclear staining of MG-63 cells cultured on (c) Ti, (d) Ti-Ag_1, (e) Ti-Ag_2, and (f) Ti-Ag_5 for 24 h. The scale bar represents 100 μm.

assay) attached to the native Ti and Ag-deposited Ti surfaces was not statistically significant (Fig. 6c–e). A slight reduction in cell attachment and spreading was evident on the Ti-Ag_5 surface (Fig. 6f). Cell differentiation, migration, and other biological phenomena at the interface decide the fate of a biomaterial.[43] Thus, adequate cell attachment and spreading of cells on the Ag-deposited Ti surface promote implant osseointegration. The Ag ions released by the deposited substrates were well tolerated by the MG-63 cells, as evidenced by the time-dependent increase in the cells.

Alkaline phosphatase (ALP) is expressed during the early stage of the osteogenic differentiation process (1–2 weeks);[44] therefore, the quantitative estimation of the ALP activity was performed at 7 and 14 days of culture. The results of the ALP activity of MG-63 osteoblasts cultured on Ti and Ag-deposited Ti samples are presented in Fig. 7a. The difference in the ALP activity between all treatment groups at 7 and 14 days was not statistically significant. Elevated ALP activity was observed in all the samples at 14 days of incubation, indicating mineralization by the actively proliferating cells. ALP plays a crucial role in bone mineralization; it catalyzes the hydrolysis of the phosphomonoester bonds at elevated pH (8–10) to liberate inorganic phosphate, which is an essential component of hydroxyapatite.[45]

Extracellular matrix (ECM) mineralization by MG-63 cells cultured on Ti and Ag-deposited samples was evaluated by applying an ARS assay. Fig. 7d–k depicts the ARS-stained monolayers of MG-63 cells after 14 and 21 days of culture on Ti and Ag-deposited Ti samples. Very few mineralized nodules (stained red) were observed on all samples after 14 days of incubation (Fig. 7d–g). However, after 21 days of culture, all the samples showed a significant amount of calcium-rich deposits (Fig. 7h–k). Among the groups, Ti and Ti-Ag_1 showed more calcium-rich deposits distributed all over the surface than Ti-Ag_2 and Ti-Ag_5. Quantitative measurements (Fig. 7b) indicated a reduction in the matrix mineralization by MG-63 cells on the Ti-Ag_2 and Ti-Ag_5 compared to the Ti and Ti-Ag_1 samples.

The expression of *ALP*, *Col1α*, *BMP-2*, and *RUNX-2* genes in MG-63 osteoblasts after 14 and 21 days of osteogenic induction on Ti and Ag-deposited Ti samples was assessed by qPCR (Fig. 8). ALP catalyzes the hydrolysis of phosphomonoesters and pyrophosphates to generate inorganic phosphate, which is a part of hydroxyapatite. BMP-2 induces the differentiation of mesenchymal stem cells into osteoblasts in early osteogenesis. Col1α synthesizes type 1 collagen, which makes up 90% of the organic component of the bone matrix. RUNX-2 is an important transcription factor that regulates the expression of different osteogenic genes.[46] We observed a statistically significant

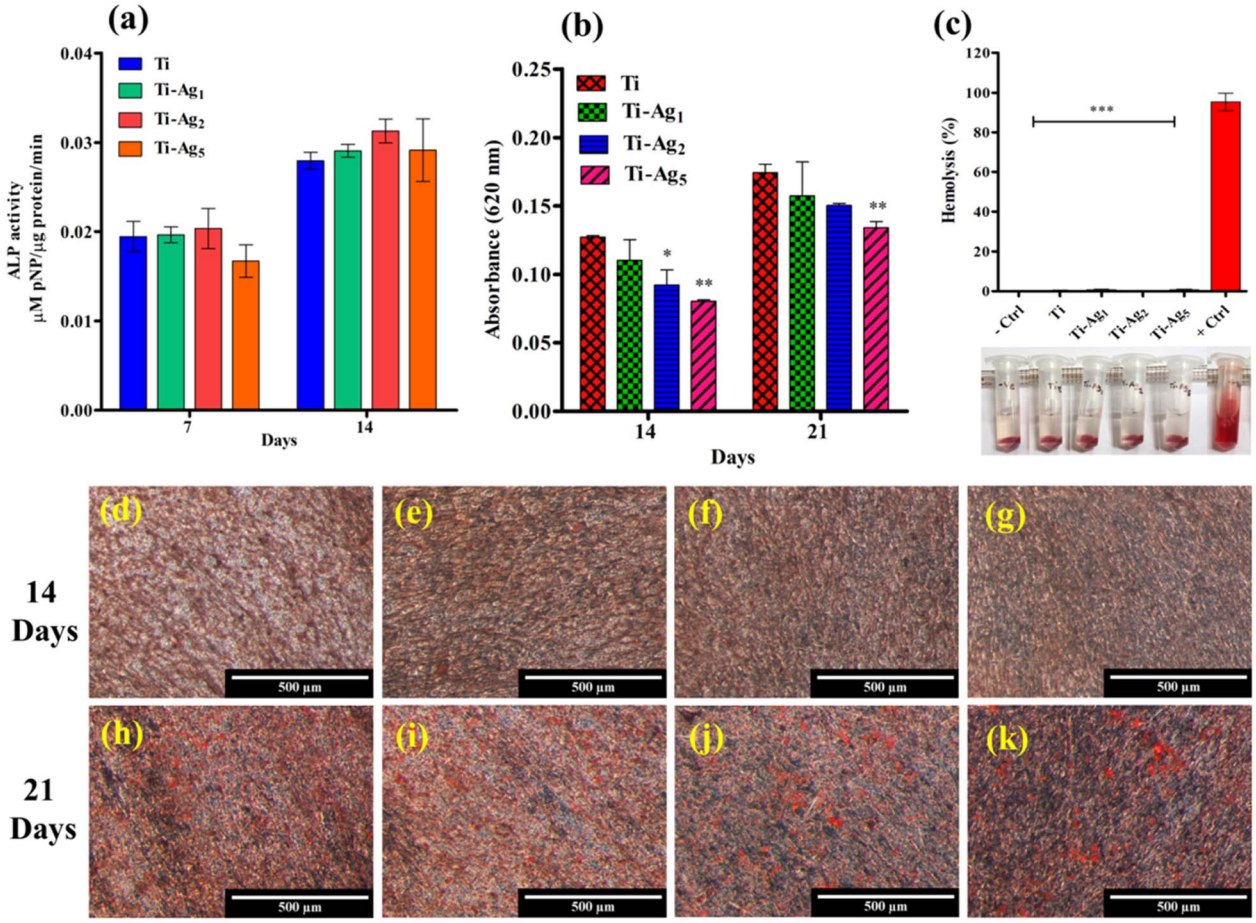

Fig. 7 (a) Determination of ALP activity. (b) Spectrophotometric estimation of the ARS dye. * indicates $p < 0.05$, ** $p < 0.01$, when compared with native Ti (control). (c) Comparison of % hemolysis between Triton X-100 (positive control), saline (negative control), Ti, and Ag-deposited Ti discs. *** indicates $p < 0.001$ when compared to the positive control. Stereomicroscopic images of ARS-stained MG-63 cell monolayer on (d) Ti, (e) Ti-Ag_1, (f) Ti-Ag_2, and (g) Ti-Ag_5 for 14 days and (h) Ti, (i) Ti-Ag_1, (j) Ti-Ag_2, and (k) Ti-Ag_5 for 21 days. The scale bar represents 500 μm.

reduction in the expression of the *ALP* gene between Ti and Ag-deposited Ti surfaces after 14 days. This reduction in ALP gene expression might be due to the excess Ag present in the culture medium during the early incubation period. However, on day 21, *ALP* gene expression was similar to that of the control Ti (Fig. 8a). At 14 and 21 days of culture, no difference in the *Col1α* gene expression between control and Ag-deposited samples was observed (Fig. 8b). Additionally, the relative gene expression of *BMP-2* was similar in the Ag-deposited and control Ti samples after 14 days. However, on day 21, the Ti-Ag_2 and Ti-Ag_5 samples showed significantly higher *BMP-2* expression ($p < 0.01$) than Ti (Fig. 8c). In the case of *RUNX-2* gene expression, the difference between the Ti and Ag-deposited Ti samples at 14 days was statistically insignificant, but on day 21, reduced gene expression was observed on the Ag-deposited Ti surfaces compared to the control (Fig. 8c). Recently, Xie *et al.* showed a reduction in *ALP*, *OCN*, and *Col1* gene expression in MG-63 cells after higher Ag NP treatment.[47] The authors observed a dose-dependent reduction in the expression of *ALP*, *OCN*, and *Col1* genes, which resulted in the inhibition of the differentiation and mineralization of osteoblasts. In conclusion, a reduction in the expression of osteogenesis-related genes of MG-63 cells on the Ti-Ag_5 surface could be attributed to Ag release from the surface, which might have interfered with the osteogenesis process. A similar reduction in the calcium-rich deposits on the Ti-Ag_5 surface was observed in the ARS assay, further substantiating the qPCR results.

3.4 Hemolysis assay

Evaluation of *in vitro* blood compatibility of the blood-contacting biomaterials is one of the preliminary criteria that biomaterials must satisfy before clinical application.[48] The adverse interaction of biomaterial with blood may lead to severe complications, such as hemolysis, coagulation, and immune rejection, ultimately resulting in implant failure.[49] A hemolysis assay was employed to assess the hemocompatibility of Ag-deposited Ti. The results of the hemolysis assay revealed <5% hemolysis using Ti and Ag-deposited Ti samples compared to Triton X-100 (positive control, complete hemolysis) (Fig. 7c). The photograph of the microcentrifuge tubes in Fig. 7c shows the blood kept in contact with the respective sample. The clear supernatant and intact RBC pellets indicate the

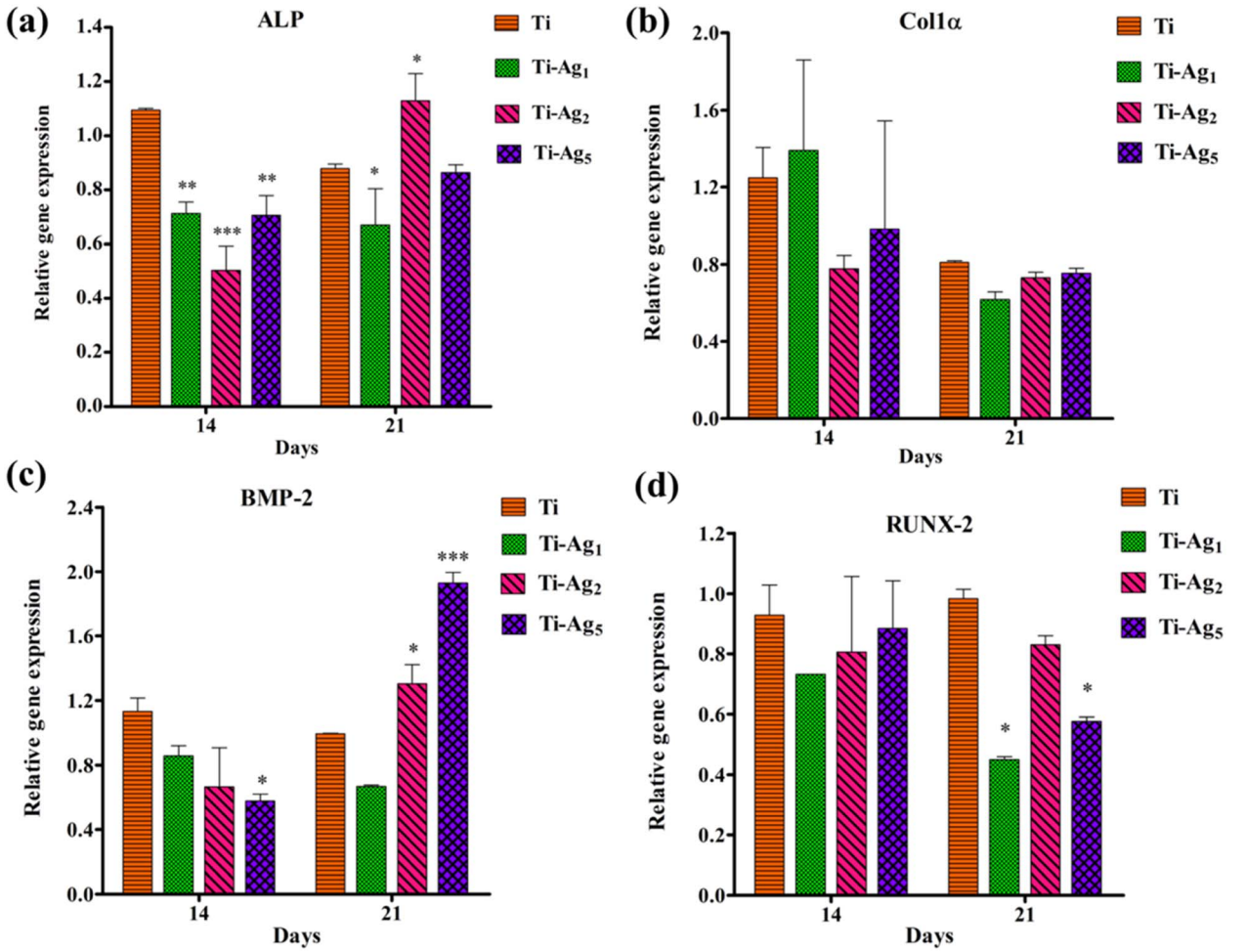

Fig. 8 Relative gene expression analysis of osteogenesis-related genes: (a) *ALP*, (b) *Col1α*, (c) *BMP-2*, and (d) *RUNX-2* in MG-63 osteoblasts cultured on Ti and Ag-deposited Ti discs for 14 and 21 days. * indicates $p < 0.05$, ** $p < 0.01$, and *** $p < 0.001$ when compared with Ti.

hemocompatibility of these samples. These data suggest that Ag-deposited Ti samples possess excellent hemocompatibility and are thus safe for *in vivo* applications.

Conventional Ti implants lack effective antimicrobial activity; therefore, in a few instances, bacterial infection during early healing leads to implant failure. One of the best strategies to avoid implant failure is the surface modification of the implant, which ensures aseptic healing and early osseointegration.[14] Implant surface modification using Ag bears an advantage over other strategies, such as antibiotics, and antimicrobial peptides, because of its strong antibacterial activity, broad antibacterial spectrum, lower bacterial resistance, and excellent stability due to its inorganic nature.[50] Earlier, the antibacterial activity and biocompatibility of Ag-coated Ti as an abutment were described.[25] Keeping this in mind, we evaluated the antibacterial potential of Ag-deposited Ti specifically against periodontal pathogens implicated in peri-implantitis. The bacteria belonging to yellow (*S. sanguinis*, *S. oralis*), purple (*A. actinomycetemcomitans*), and red (*P. gingivalis*, *P. gingivalis 93* (Indian strain)) complexes were specifically chosen to represent the predominant genera during infections. Deposition of Ag resulted in the formation of nanoscale topography on the Ti surface, which increased the surface wettability and SFE of native Ti; this is similar to the observations by Kim *et al.*[51] Furthermore, as reported by Parisi *et al.* and Lin *et al.*, hydrophilic Ti surfaces with higher SFE adsorb more fibronectin (a component of ECM, which interacts with integrin on the cell surface) and enhance cell attachment, spreading, proliferation, and differentiation, which help in early osseointegration.[52,53] In the early period after implant placement, the burst release of Ag essentially curbs the bacterial infection. After this, once the surgery site is healed and primary osseointegration is completed, continued Ag release, albeit at a low level, and the host immune response are sufficient to ensure no bacterial infections in the subsequent stages.[50] Thus, the coating of Ag ensures long-term maintenance of aseptic conditions not only during the early healing period but also for up to three weeks, which is extremely meaningful for *in vivo* application. Among the all deposited groups, the Ti-Ag_5 sample showed excellent antibacterial activity against periodontal pathogens under *in vitro* experiments, which is similar to the earlier findings.[54,55] SEM analysis clearly showed bacterial cell

damage on Ti-Ag_5 samples hinting toward contact and release-mediated killing of bacteria by Ag ions.[55] Strain-dependent antimicrobial activity is reported in earlier studies; this probably explains the effectiveness of Ti-Ag_5 surfaces than the Ti-Ag_1 and Ti-Ag_2 against periodontal pathogens.

Healthy interaction between the biomaterial and surrounding tissue plays a significant role in successful biointegration. In particular, early osteoblast attachment, proliferation, and differentiation allow hard tissue formation around the implant without intervening in soft tissue, which ultimately determines the success of the osseointegration. Although the antibacterial property is essential, it must not come at the cost of adverse biocompatibility; therefore, the effect of Ag coating on the bioactivities of MG-63 osteoblasts was assessed.[47,56] All Ag-deposited Ti groups showed good cytocompatibility and no adverse effect on cell proliferation activity. It has been reported that Ag at lower concentrations is completely safe for the cells; however, at higher concentrations, it induces cell membrane damage, oxidative stress, protein/DNA binding and damage, and apoptotic cell death.[54] ALP is an early marker of osteogenesis, and its normal expression is very important in bone formation. No significant difference in ALP activity was observed compared to native Ti at 7 and 14 days, indicating its suitability for *in vivo* application. *In vitro*, a calcium deposition assay helps to gain insight into the biomineralization process. Results of the ARS and qPCR assays indicated that Ti-Ag_5 surfaces supported lower levels of calcium deposition and a reduction in osteogenesis gene expression. At best, this could be ascribed to a marginal decrease in the osteoblast bioactivity attributed to the Ag released from Ti-Ag_5 surfaces than the Ti-Ag_1 and Ti-Ag_2.[47] The biocompatibility of developed materials and *in vitro* cellular responses depend on the cell types (*ca.* established cells such as osteoblasts and osteoclasts, and primary cells derived from host tissue), which are used for assays.[57] The presence of a very low quantity of Ag (not exceeding 5 μg mL^{-1}) over a long time was reported to have a positive effect on the cell viability and the expression of osteogenesis-related genes in the BMSCs.[57] These results are in line with our data and prove that Ag-deposited Ti possesses excellent antibacterial activity and good cytocompatibility. However, *in vivo* studies are warranted for successful clinical applications.

4. Conclusion

In summary, as an extension of our previous study, we successfully deposited Ag on the Ti disc using DC sputtering. Ag-deposited Ti samples exhibited a reduction in surface roughness and an improvement in wettability and SFE. The Ag-deposited Ti samples, especially Ti-Ag_5, showed complete inhibition of periodontal pathogens implicated in peri-implantitis. Moreover, the Ag-deposited Ti samples did not exhibit an adverse effect on the cell viability, proliferation behavior, and ALP activity of the MG-63 osteoblast. The marginal reduction in the calcium mineralization and expression of osteogenesis-related genes observed in the Ag-deposited Ti samples was probably a cell-line-dependent observation. Taken together, it can be concluded that Ag surface modification of Ti using DC sputtering could be a promising approach for the successful osseointegration of Ti implants.

Data availability

Data will be made available on request.

Author contributions

Vaibhav Madiwal: methodology, formal analysis, writing – original draft preparation; Jyutika Rajwade: conceptualization, methodology, supervision, validation, analysis, resources, writing – review & editing.

Conflicts of interest

The authors declare no competing financial interests.

Acknowledgements

The authors acknowledge the facilities provided by Director, Agharkar Research Institute, Pune, for conducting the research. VM availed research fellowship from University Grants Commission (Award No.: 454 20/12/2015(ii)EU-V). The graphical abstract was prepared using **https://BioRender.com**.

References

1 C. Glücker, A. Rauch and S. Hahnel, Attitude and treatment options in implantsupported prosthetics: a survey among a cohort of German dentists, *J. Adv. Prosthodont*, 2020, **12**, 15–21, DOI: **10.4047/jap.2020.12.1.15**.

2 V. Moraschini, L. A. D. C. Poubel, V. F. Ferreira and E. D. S. P. Barboza, Evaluation of survival and success rates of dental implants reported in longitudinal studies with a follow-up period of at least 10 years: a systematic review, *Int. J. Oral Maxillofac. Surg.*, 2015, **44**, 377–388, DOI: **10.1016/j.ijom.2014.10.023**.

3 H. Dreyer, J. Grischke, C. Tiede, J. Eberhard, A. Schweitzer, S. E. Toikkanen, S. Glöckner, G. Krause and M. Stiesch, Epidemiology and risk factors of peri-implantitis: a systematic review, *J. Periodontal Res.*, 2018, **53**, 657–681, DOI: **10.1111/jre.12562**.

4 H. Chouirfa, H. Bouloussa, V. Migonney and C. Falentin-Daudré, Review of titanium surface modification techniques and coatings for antibacterial applications, *Acta Biomater.*, 2019, **83**, 37–54, DOI: **10.1016/j.actbio.2018.10.036**.

5 G. R. Persson and S. Renvert, Cluster of bacteria associated with peri-implantitis, *Clin. Implant Dent. Relat. Res.*, 2014, 783–793, DOI: **10.1111/cid.12052**.

6 F. T. I. Sanz-Martin, J. Doolittle-Hall, R. P. Teles, M. Pate, G. N. Belibasakis, C. H. Hämmerle and R. E. Jung, Exploring the microbiome of healthy and diseased peri-implant sites using Illumina Sequencing, *J. Clin. Periodontol.*, 2017, **44**, 1274–1284, DOI: **10.1111/jcpe.12788**.

7 G. N. Belibasakis, Microbiological and immuno-pathological aspects of peri-implant diseases, *Arch. Oral Biol.*, 2014, **59**, 66–72, DOI: 10.1016/j.archoralbio.2013.09.013.

8 R. López-Píriz, B. Cabal, L. Goyos-Ball, A. Fernández, J. F. Bartolomé, J. S. Moya and R. Torrecillas, Current state-of-the-art and future perspectives of the three main modern implant-dentistry concerns: aesthetic requirements, mechanical properties, and peri-implantitis prevention, *J. Biomed. Mater. Res., Part A*, 2019, 1466–1475, DOI: 10.1002/jbm.a.36661.

9 J. H. Fu and H. L. Wang, Breaking the wave of peri-implantitis, *Periodontol*, 2000, **84**, 145–160, DOI: 10.1111/prd.12335.

10 L. Chen, S. Komasa, Y. Hashimoto, S. Hontsu and J. Okazaki, In vitro and in vivo osteogenic activity of titanium implants coated by pulsed laser deposition with a thin film of fluoridated hydroxyapatite, *Int. J. Mol. Sci.*, 2018, **19**, 1127, DOI: 10.3390/ijms19041127.

11 S. Spriano, S. Yamaguchi, F. Baino and S. Ferraris, A critical review of multifunctional titanium surfaces: new frontiers for improving osseointegration and host response, avoiding bacteria contamination, *Acta Biomater.*, 2018, **79**, 1–22, DOI: 10.1016/j.actbio.2018.08.013.

12 X. D. Sun, T. T. Liu, Q. Q. Wang, J. Zhang and M. S. Cao, Surface modification and functionalities for titanium dental implants, *ACS Biomater. Sci. Eng.*, 2023, **9**, 4442–4461, DOI: 10.1021/acsbiomaterials.3c00183.

13 S. Kligman, Z. Ren, C. H. Chung, M. A. Perillo, Y. C. Chang, H. Koo, Z. Zheng and C. Li, The impact of dental implant surface modifications on osseointegration and biofilm formation, *J. Clin. Med.*, 2021, **10**, 1641, DOI: 10.3390/jcm10081641.

14 G. Zhu, G. Wang and J. J. Li, Advances in implant surface modifications to improve osseointegration, *Mater. Adv.*, 2021, **2**, 6901–6927, DOI: 10.1039/d1ma00675d.

15 S. Kheur, M. Kheur, V. Madiwal, R. Sandhu, T. Lakha, J. Rajwade, T. F. Eyüboğlu and M. Özcan, In-Vitro Evaluation of Photofunctionalized Implant Surfaces in a High-Glucose Microenvironment Simulating Diabetics, *J. Funct. Biomater.*, 2023, **14**, 130, DOI: 10.3390/jfb14030130.

16 R. Bai, L. Peng, Q. Sun, Y. Zhang, L. Zhang, Y. Wei and B. Han, Metallic antibacterial surface treatments of dental and orthopedic materials, *Materials*, 2020, **13**, 1–21, DOI: 10.3390/ma13204594.

17 J. Butler, R. D. Handy, M. Upton and A. Besinis, Review of Antimicrobial Nanocoatings in Medicine and Dentistry: Mechanisms of Action, Biocompatibility Performance, Safety, and Benefits Compared to Antibiotics, *ACS Nano*, 2022, **17**, 7064–7092, DOI: 10.1021/acsnano.2c12488.

18 J. A. Lenis, P. Rico, J. L. G. Ribelles, M. A. Pacha-Olivenza, M. L. González-Martín and F. J. Bolívar, Structure, morphology, adhesion and in vitro biological evaluation of antibacterial multi-layer HA-Ag/SiO2/TiN/Ti coatings obtained by RF magnetron sputtering for biomedical applications, *Mater. Sci. Eng., C*, 2020, **116**, 111268, DOI: 10.1016/j.msec.2020.111268.

19 D. M. Mihut, A. Afshar, L. W. Lackey and K. N. Le, Antibacterial effectiveness of metallic nanoparticles deposited on water filter paper by magnetron sputtering, *Surf. Coat. Technol.*, 2019, **368**, 59–66, DOI: 10.1016/j.surfcoat.2019.04.039.

20 S. Ippili, V. Jella, J. M. Lee, J. S. Jung, D. H. Lee, T. Y. Yang and S. G. Yoon, ZnO-PTFE-based antimicrobial, anti-reflective display coatings and high-sensitivity touch sensors, *J. Mater. Chem. A*, 2022, **10**, 22067–22079, DOI: 10.1039/d2ta06095g.

21 Q. Nawaz, S. Fastner, M. A. U. Rehman, S. Ferraris, S. Perero, G. G. di Confiengo, E. Yavuz, M. Ferraris and A. R. Boccaccini, Multifunctional stratified composite coatings by electrophoretic deposition and RF co-sputtering for orthopaedic implants, *J. Mater. Sci.*, 2021, **56**, 7920–7935, DOI: 10.1007/s10853-020-05725-w.

22 I. Lampé, D. Beke, S. Biri, I. Csarnovics, A. Csik, Z. Dombrádi, P. Hajdu, V. Hegedűs, R. Rácz, I. Varga and C. Hegedűs, Investigation of silver nanoparticles on titanium surface created by ion implantation technology, *Int. J. Nanomed.*, 2019, **14**, 4709–4721, DOI: 10.2147/IJN.S197782.

23 S. yi Shao, J. xi Chen, H. yan Tang, P. pan Ming, J. Yang, W. qing Zhu, S. mei Zhang and J. Qiu, A titanium surface modified with zinc-containing nanowires: enhancing biocompatibility and antibacterial property in vitro, *Appl. Surf. Sci.*, 2020, **515**, 146107, DOI: 10.1016/j.apsusc.2020.146107.

24 R. Liu, K. Memarzadeh, B. Chang, Y. Zhang, Z. Ma, R. P. Allaker, L. Ren and K. Yang, Antibacterial effect of copper-bearing titanium alloy (Ti-Cu) against Streptococcus mutans and Porphyromonas gingivalis, *Sci. Rep.*, 2016, **6**, 1–10, DOI: 10.1038/srep29985.

25 S. Kheur, N. Singh, D. Bodas, J. Y. Rauch, S. Jambhekar, M. Kheur and J. Rajwade, Nanoscale silver depositions inhibit microbial colonization and improve biocompatibility of titanium abutments, *Colloids Surf., B*, 2017, **159**, 151–158, DOI: 10.1016/j.colsurfb.2017.07.079.

26 D. Hong, K. E. Bae, S. P. Hong, J. H. Park, I. S. Choi and W. K. Cho, Mussel-inspired, perfluorinated polydopamine for self-cleaning coating on various substrates, *Chem. Commun.*, 2014, **50**, 11649–11652, DOI: 10.1039/c4cc02775b.

27 S. Rashid, M. Sebastiani, M. Z. Mughal, R. Daniel and E. Bemporad, Influence of the silver content on mechanical properties of Ti-Cu-Ag thin films, *Nanomaterials*, 2021, **11**, 1–14, DOI: 10.3390/nano11020435.

28 R. Wan, X. Wang, L. Lei, G. Hu, H. Tang and H. Gu, Enhanced anti-microbial activity and osseointegration of Ta/Cu co-implanted polyetheretherketone, *Colloids Surf., B*, 2022, **218**, 112719, DOI: 10.1016/j.colsurfb.2022.112719.

29 K. J. Livak and T. D. Schmittgen, Analysis of relative gene expression data using real-time quantitative PCR and the 2-ΔΔCT method, *Methods*, 2001, **25**, 402–408, DOI: 10.1006/meth.2001.1262.

30 G. Patil, R. Pawar, S. Jadhav and V. Ghormade, A chitosan based multimodal "soft" hydrogel for rapid hemostasis of non-compressible hemorrhages and its mode of action,

Carbohydr. Polym. Technol. Appl., 2022, **4**, 100237, DOI: 10.1016/j.carpta.2022.100237.

31 W. Qian, L. Gong, X. Cui, Z. Zhang, A. Bajpai, C. Liu, A. B. Castillo, J. C. M. Teo and W. Chen, Nanotopographic Regulation of Human Mesenchymal Stem Cell Osteogenesis, *ACS Appl. Mater. Interfaces*, 2017, **9**, 41794–41806, DOI: 10.1021/acsami.7b16314.

32 S. Cai, C. Wu, W. Yang, W. Liang, H. Yu and L. Liu, Recent advance in surface modification for regulating cell adhesion and behaviors, *Nanotechnol. Rev.*, 2020, **9**, 971–989, DOI: 10.1515/ntrev-2020-0076.

33 J. Tang, Z. Wu, X. Yao, Y. Zhou, Y. Xiong, Y. Li, J. Xu, M. S. Dargusch and M. Yan, From bio-inertness to osseointegration and antibacterial activity: a one-step micro-arc oxidation approach for multifunctional Ti implants fabricated by additive manufacturing, *Mater. Des.*, 2022, **221**, 110962, DOI: 10.1016/j.matdes.2022.110962.

34 H. Fan and Z. Guo, Bioinspired surfaces with wettability: biomolecule adhesion behaviors, *Biomater. Sci.*, 2020, **8**, 1502–1535, DOI: 10.1039/c9bm01729a.

35 M. Bartmański, Ł. Pawłowski, G. Strugała, A. Mielewczyk-Gryń and A. Zieliński, Properties of nanohydroxyapatite coatings doped with nanocopper, obtained by electrophoretic deposition on Ti13Zr13Nb alloy, *Materials*, 2019, **12**, 3741, DOI: 10.3390/ma12223741.

36 J. A. Otte, J. Zou, R. Patel, M. Lu and M. S. Dargusch, Tib nanowhisker reinforced titanium matrix composite with improved hardness for biomedical applications, *Nanomaterials*, 2020, **10**, 1–11, DOI: 10.3390/nano10122480.

37 A. S. Abdullah, M. N. Mohd Nawi, M. A. Othuman Mydin, M. W. Sari, R. Ahmad and M. M. A. B. Abdullah, The Significant Effect of Mechanical Treatment on Ceramic Coating for Biomedical Application, *Materials*, 2022, **15**, 6550, DOI: 10.3390/ma15196550.

38 K. Wu, Y. Yang, Y. Zhang, J. Deng and C. Lin, A ntimicrobial activity and cytocompatibility of silver nanoparticles coated catheters via a biomimetic surface functionalization strategy, *Int. J. Nanomed.*, 2015, **10**, 7241–7252, DOI: 10.2147/IJN.S92307.

39 R. Lotha, B. R. Shamprasad, N. Sri, R. Ganapathy, S. Nagarajan and A. Sivasubramanian, Microbial Pathogenesis Zero valent silver nanoparticles capped with capsaicinoids containing Capsicum annuum extract , exert potent anti-bio fi lm e ff ect on food borne pathogen Staphylococcus aureus and curtail planktonic growth on a zebra fi sh infection model, *Microb. Pathog.*, 2018, **124**, 291–300, DOI: 10.1016/j.micpath.2018.08.053.

40 Y. Qing, L. Cheng, R. Li, G. Liu, Y. Zhang, X. Tang, J. Wang, H. Liu and Y. Qin, Potential antibacterial mechanism of silver nanoparticles and the optimization of orthopedic implants by advanced modification technologies, *Int. J. Nanomed.*, 2018, **13**, 3311–3327, DOI: 10.2147/IJN.S165125.

41 Y. Si, H. Liu, H. Yu, X. Jiang and D. Sun, MOF-derived CuO@ZnO modified titanium implant for synergistic antibacterial ability, osteogenesis and angiogenesis, *Colloids Surf., B*, 2022, **219**, 112840, DOI: 10.1016/j.colsurfb.2022.112840.

42 S. Mukherjee, S. Sharma, V. Soni, A. Joshi, A. Gaikwad, J. Bellare and J. Kode, Improved osteoblast function on titanium implant surfaces coated with nanocomposite Apatite–Wollastonite–Chitosan– an experimental in-vitro study, *J. Mater. Sci.: Mater. Med.*, 2022, **33**, 25, DOI: 10.1007/s10856-022-06651-w.

43 J. Sun, D. Wei, K. Yang, Y. Yang, X. Liu, H. Fan and X. Zhang, The development of cell-initiated degradable hydrogel based on methacrylated alginate applicable to multiple microfabrication technologies, *J. Mater. Chem. B*, 2017, **5**, 8060–8069, DOI: 10.1039/c7tb01458a.

44 F. Westhauser, M. Karadjian, C. Essers, A. S. Senger, S. Hagmann, G. Schmidmaier and A. Moghaddam, Osteogenic differentiation of mesenchymal stem cells is enhanced in a 45S5-supplemented β-TCP composite scaffold: an in-vitro comparison of Vitoss and Vitoss BA, *PLoS One*, 2019, **14**, 1–18, DOI: 10.1371/journal.pone.0212799.

45 S. Vimalraj, Alkaline phosphatase: structure, expression and its function in bone mineralization, *Gene*, 2020, **754**, 144855, DOI: 10.1016/j.gene.2020.144855.

46 Y. Ding, Z. Yuan, P. Liu, K. Cai and R. Liu, Fabrication of strontium-incorporated protein supramolecular nanofilm on titanium substrates for promoting osteogenesis, *Mater. Sci. Eng., C*, 2020, **111**, 110851, DOI: 10.1016/j.msec.2020.110851.

47 H. Xie, P. Wang and J. Wu, Effect of exposure of osteoblast-like cells to low-dose silver nanoparticles: uptake, retention and osteogenic activity, *Artif. Cells, Nanomed., Biotechnol.*, 2019, **47**, 260–267, DOI: 10.1080/21691401.2018.1552594.

48 M. Weber, H. Steinle, S. Golombek, L. Hann, C. Schlensak, H. P. Wendel and M. Avci-Adali, Blood-Contacting Biomaterials: In Vitro Evaluation of the Hemocompatibility, *Front. Bioeng. Biotechnol.*, 2018, **6**, 99, DOI: 10.3389/fbioe.2018.00099.

49 P. Ou, T. Zhang, J. Wang, C. Li, C. Shao and J. Ruan, Bone response in vivo of Ti-45Zr alloy as dental implant material, *J. Mater. Sci.: Mater. Med.*, 2022, **33**, 47, DOI: 10.1007/s10856-022-06664-5.

50 L. Zhao, H. Wang, K. Huo, L. Cui, W. Zhang, H. Ni, Y. Zhang, Z. Wu and P. K. Chu, Antibacterial nano-structured titania coating incorporated with silver nanoparticles, *Biomaterials*, 2011, **32**, 5706–5716, DOI: 10.1016/j.biomaterials.2011.04.040.

51 S. Kim, C. Park, K. H. Cheon, H. Do Jung, J. Song, H. E. Kim and T. S. Jang, Antibacterial and bioactive properties of stabilized silver on titanium with a nanostructured surface for dental applications, *Appl. Surf. Sci.*, 2018, **451**, 232–240, DOI: 10.1016/j.apsusc.2018.04.270.

52 L. Parisi, B. Ghezzi, M. G. Bianchi, A. Toffoli, F. Rossi, O. Bussolati and G. M. Macaluso, Titanium dental implants hydrophilicity promotes preferential serum fibronectin over albumin competitive adsorption modulating early cell response, *Mater. Sci. Eng., C*, 2020, **117**, 111307, DOI: 10.1016/j.msec.2020.111307.

53 J. Lin, H. Dong, Y. Wen, X. Zhuang and S. Li, Surface Free Energy of Titanium Disks Enhances Osteoblast Activity by

Affecting the Conformation of Adsorbed Fibronectin, *Front. Mater.*, 2022, **9**, 1–11, DOI: **10.3389/fmats.2022.840813**.

54 R. Pokrowiecki, T. Zaręba, B. Szaraniec, K. Pałka, A. Mielczarek, E. Menaszek and S. Tyski, In vitro studies of nanosilver-doped titanium implants for oral and maxillofacial surgery, *Int. J. Nanomed.*, 2017, **12**, 4285–4297, DOI: **10.2147/IJN.S131163**.

55 S. Mei, H. Wang, W. Wang, L. Tong, H. Pan, C. Ruan, Q. Ma, M. Liu, H. Yang, L. Zhang, Y. Cheng, Y. Zhang, L. Zhao and P. K. Chu, Antibacterial effects and biocompatibility of titanium surfaces with graded silver incorporation in titania nanotubes, *Biomaterials*, 2014, **35**, 4255–4265, DOI: **10.1016/j.biomaterials.2014.02.005**.

56 A. Radtke, M. Grodzicka, M. Ehlert, T. Jędrzejewski, M. Wypij and P. Golińska, To be Microbiocidal and not to be Cytotoxic at the same time —Silver Nanoparticles and their main role on the Surface of Titanium Alloy Implants, *J. Clin. Med.*, 2019, **8**, 334, DOI: **10.3390/jcm8030334**.

57 D. Li, Y. Qiu, S. Zhang, M. Zhang, Z. Chen and J. Chen, A Multifunctional Antibacterial and Osteogenic Nanomedicine: QAS-Modified Core-Shell Mesoporous Silica Containing Ag Nanoparticles, *BioMed Res. Int.*, 2020, **2020**, 4567049, DOI: **10.1155/2020/4567049**.